NUMERICAL AND EXPERIMENTAL STUDY ON WAVE PROPAGATION IN THE OPEN ATMOSPHERE

(Date received: 25.03.12/Date accepted: 24.11.12)

Mohammad Ali Jinnah[1] and Mohammad Monjurul Ehsan[2]

MCE Department, Islamic University of Technology (IUT),
Board Bazar, Gazipur-1704, Bangladesh
E-mail: [1]jinnah@iut-dhaka.edu, [2]mme.ehsan@gmail.com

ABSTRACT

In the present research works, wave propagation in the open atmosphere has been investigated both numerically and experimentally. Two-dimensional (2D) numerical code has been developed to solve the Euler equations for the upstream and downstream parameters during the shock wave propagation in the open atmosphere. It is observed that due to decay of the shock strength, all parameters (velocity, pressure and density) in the upstream of the shock wave are decreased as increasing the travel time of the wave in the open atmosphere. It is seen from the numerical images that the propagation of the shock front in the open atmosphere is spherical in shape. An experiment has been conducted by a horizontal shock tube to generate subsonic wave as well as shock wave with supersonic speed by rupturing different types of diaphragms. The properties of diaphragm are the major factors to generate shock wave in the shock tube. It is observed that the properties of diaphragm like toughness and brittleness are the best properties in the present case. In the present experiment, transparent Raksin sheet and used X-ray film are selected as the diaphragm where used X-ray film has the better rupturing quality as compare to Raksin sheet. For measuring the wave speed, a time measuring technique has been developed to measure the wave travel time in the open atmosphere and it is simple in use and accurate in measurement as compare to other complicated technique like wave visualization by High Speed Video camera. During the wave propagation in the open atmosphere, the wave speed decreases and the decay of the wave strength is observed.

Keywords: *Euler equations, Open Atmosphere, Shock wave, Wave decay, Wave visualization*

1.0 INTRODUCTION

For the study of wave propagation in the open atmosphere, an experiment has been conducted to measure the wave speed during the propagation in the open atmosphere. The measurement of wave speed and the determination of its location in the open atmosphere is one of the complex experimental works in the laboratory. In the present research works, a technique has been developed to measure the wave propagation time between two locations and it is very simple in use and accurate in measurement as compare to other existing methods. The measurement of the wave speed is used to investigate the decay of the wave strength as well as the decay of the shock wave strength in the open atmosphere. Both experimental and numerical investigation is essential to improve the understanding of the decay phenomena of the shock strength during interaction with objects in the open atmosphere. A numerical code has been developed to solve the Euler equations for the non-viscous flow field in the open atmosphere and the present code is one of the modified versions of the code developed by Jinnah and Takayama [1]. Many researchers had been used optical techniques to visualize the wave propagation for measuring the wave speed and the location of the wave. Widely used qualitative and semi-quantitative optical flow diagnostics are shadowgraph, schlieren, and interferometry but the application of some of these techniques to supersonic and hypersonic flows can be highly challenging due to the high velocity, strong gradients and restricted optical access generally encountered. Doig *et al.* [2] conducted experiment where direction-indicating color schlieren flow visualization was used to determine optically the general effectiveness of the methods. Multiple images were taken during a single tunnel run, which allowed, to some extent, confirmation of the general steadiness of the flow.

Laser-based techniques such as laser Doppler anemometry and particle image velocimetry are well established for investigation of supersonic flows, but as yet their use in hypersonic flows has been limited. Other relevant measurement techniques include particle tracking velocimetry, Doppler global velocimetry, laser-two-focus anemometry, background oriented schlieren and laser induced fluorescence methods, molecular tagging velocimetry for velocity measurement and thermo-graphic phosphor thermometry for surface temperature measurement. Laser measurement techniques are becoming more commonly applied to many areas of thermo-fluids and heat transfer. An area of their application, which presents highly challenging requirements, is in the measurement of aerospace flows. High speed camera can also be used for the flow visualization to analysis the structure of the wave. In the shock wave research laboratory, Tohoku University Japan, the speed of projectile was measured by Shimadzu's HPV-1 High Speed Video Camera.

In the study of metal-high explosive detonation wave interaction, by the pin technique, it was desirable to obtain time measurements to an accuracy of less than 1 microsecond (*μsec*) over a total time interval of 5 *μsec*. Commercial instruments capable of a high degree of time resolution were not available and a special instrument was developed for this purpose. Kobiera *et al*. [3] conducted experiment on the shock wave propagation through the test section and the shock wave causes a disturbance of the droplets; this process was visualized by a schlieren system and recorded by a high-speed camera. Pianthong *et al*. [4] conducted experiment with the use of the shadowgraph method, showing the projectile traveling inside and leaving the pressure relief section at a velocity of about 1100 *m/s*.

In the present method, a logic circuit has been developed to detect the metal to metal touch pulses for triggering which is finally used to open and close the gate to allow and stop the crystal frequency for counting. Using the number of pulse counted, the traveling time between the trigger points is calculated for the subsonic or supersonic objects. Normally the propagation time of the logic gates is not more then 20 nanoseconds, so the accuracy level of the measured time by the present technique will be less then 0.006%. The obtained experimental results are compared with the numerical results by solving the Euler equations for shock wave propagation in the open atmosphere and it is observed that the simulation results are satisfactory for the wave propagation in the open atmosphere. The present numerical technique can be used for designing aero-mechanism system such as supersonic aircraft by determining the shock wave interaction effects with objects and its decay phenomena during propagation in the open atmosphere.

2.0 EXPERIMENTAL SETUP

Experiments are carried out in a single diaphragm horizontal shock tube in the Fluid Mechanics Laboratory of the Islamic University of Technology (IUT). Figure 1 shows a schematic illustration of the horizontal shock tube consisting of 150 *mm* diameter and 1.5 *m* long high pressure chamber made of mild steel. High pressure chamber is the driver section of the shock tube and the driven section of the shock tube is 100 *mm* diameter and 5 *m* long. A diaphragm is used between two flanges of the driver section and the driven section of the shock tube and

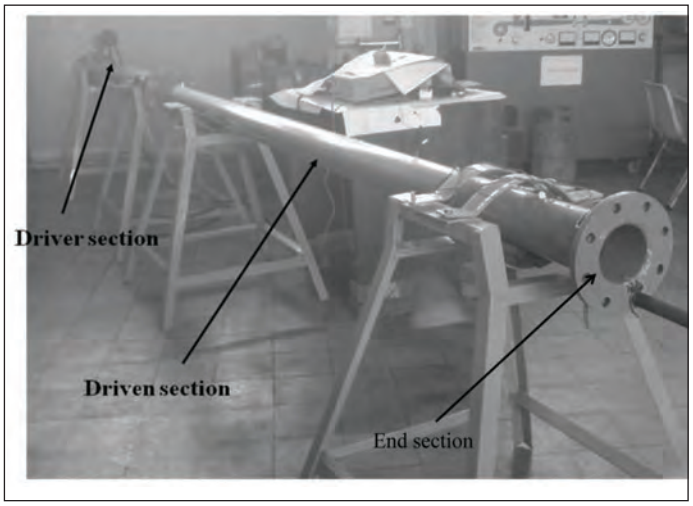

Figure 1: Simple shock tube photograph, constructed in Fluid Mechanics Lab on IUT where driver section and driven section are shown

Figure 2: Photograph of post-shocked high speed air delivered from end section of the shock tube

tightly fastens by nut-bolt with proper gasket. The diaphragm is separated the high pressure chamber from atmospheric pressure. Inserting the air (or N_2) pressure inside the high pressure chamber, chamber pressure gradually increases and due to high pressure of the chamber, the diaphragm feels tension force and at certain instant it starts rupture. Due to sudden rupture, the fluid from the high pressure chamber starts to flow with high velocity and when the flow velocity reaches to exceed sonic limit, the shock wave generates after travelling certain distance in the driven section. In the present experiment, the shock wave is allowed to propagate in the open atmosphere, even though it is not safe for human beings if the shock wave strength overcomes the moderate Mach number. After propagating the shock wave in the open atmosphere, the post-shocked high speed air delivered from the end section of the shock tube, which is shown in Figure 2. High pressure fluid, whose pressure is less than chamber pressure, drives the shock front. The rupture of the diaphragm in the shock tube depends on the diaphragm properties and it is observed that better toughness, slightly brittle property of the diaphragm can able to generate stronger shock wave. On the other hand, in smaller diameter shock tubes, diaphragms are ruptured relatively uniform and quickly and then incident shock formation distance is relatively short and its

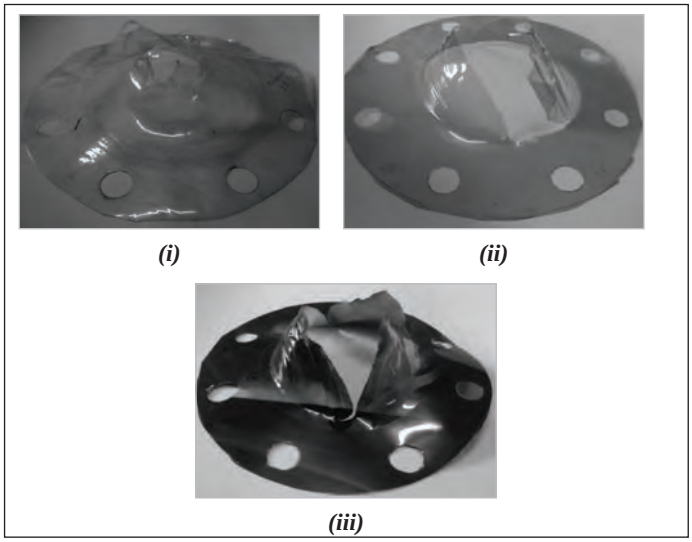

Figure 3: Rupturing characteristics of different diaphragms of (i) Thick polythene; (ii) Raksin; (iii) Used X-ray film

frontal shape is planar. However, in a large size shock tube under study, large diameter plastic diaphragm such as Mylar ones tend to rupture non-uniformly to generate three dimensionally distorted shock fronts. In the present experiment, three types of diaphragm are used where ductile typed thick polythene diaphragm is not suitable to generate shock wave. Raksin sheet and used X-ray film are suitable to use as a diaphragm for generating shock wave in the driven section of the shock tube. Rupturing characteristics of different diaphragms are observed in the experiments which are shown in Figures 3(i)-(iii). Ductile typed thick polythene diaphragm starts continuous deformation as increasing the chamber pressure and it is continuing to deform upto the rupturing of the diaphragm. So such types of diaphragm rupturing fail to create supersonic velocity suddenly at the driven section which finally does not generate shock wave. Due to toughness and brittleness of the Raksin sheet and used X-ray film, the deformation is not linear as increasing the chamber pressure and the rupturing happened suddenly making large ruptured area. Due to sudden diaphragm ruptured, a fluid column from high pressure chamber starts to move through driven section and creates shock wave after travelling certain distance in the driven section. At the same time, an expansion wave, known as expansion fan, moves through high pressure chamber, as a result, a contact surface is created which is moved behind the shock wave with lower velocity, as shown in Figure 4. Figure 4 gives an *x-t* diagram for a typical shock wave indicating the available test time in the test section of the shock tube. The test time is terminated by the arrival of the reflected expansion wave head from the driver end as indicated in Figure 4 and the arrival of the contact surface terminates the test time for the reflection of the incident shock waves from the driven end section if the end wall present at the end section. In the present case, the incident wave propagates in the open atmosphere from the driven end section because of the absence of the end wall.

In the present experiment, the constructed shock tube is used to generate shock wave at the outlet of the shock tube. The chamber pressure of the shock tube is taken in the range of 3.5 – 4.5 kg/cm^2 and due to sudden rupture of the diaphragm, a wave generates in the shock tube which travels with subsonic or supersonic speed depending on the pressure inside the chamber during rupturing. If the chamber pressure increases, a shock wave generates after diaphragm rupturing. A time measuring device is

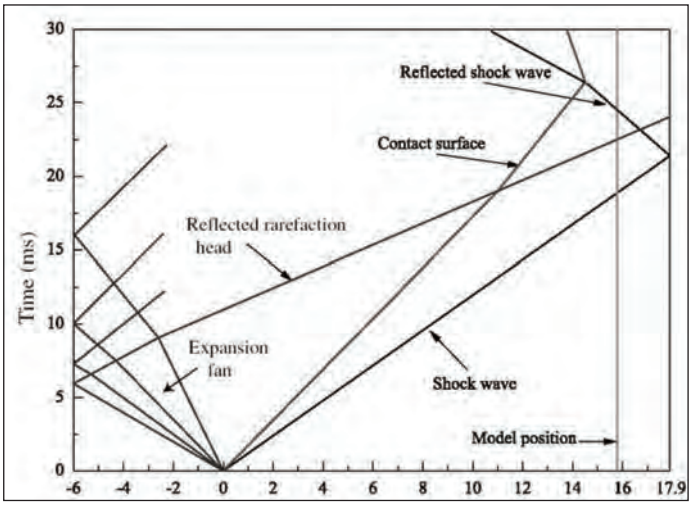

Figure 4: A typical x-t diagram for the relative direction of the shock wave and expansion wave propagation after the rupture of diaphragm

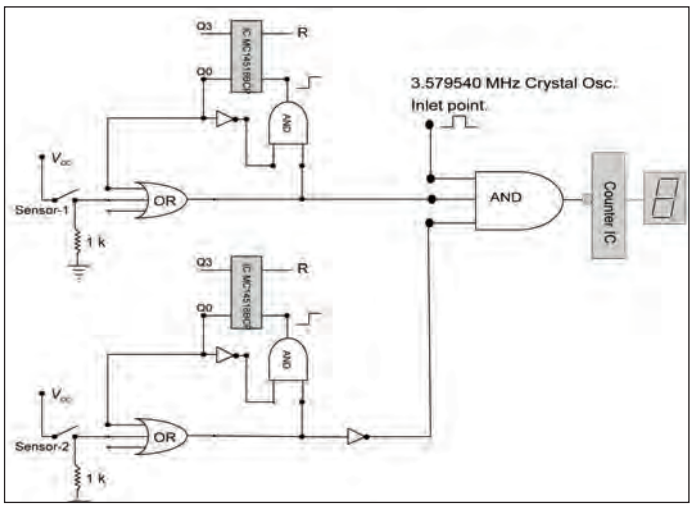

Figure 5: Circuit layout use to construct time measuring device

used to measure the travel time of the wave propagation in the open atmosphere. The logic circuit for the time measuring device has been developed by using two sensing points as shown in Figure 5. In sensing point-1, a metal wire carrying sufficient voltage when touches another metal wire then a voltage signal generates in that wire which causes to change the state of the AND gate to open and allow to pass the crystal frequency through it. Similarly in sensing point-2, shown in Figure 5, a digital signal closes the AND gate not to pass the crystal frequency through it. In this sensing technique, a direct metal to metal contact sensing is more efficient as compare to other sensing devices, like pressure transducers, Electro-optic sensors, Infrared sensors, Magnetic sensors etc and here is not necessary to change the signal, like light, heat, magnetic signal into electric voltage signal. Using the number of pulse counted, the traveling time of the wave between two sensing points is calculated.

Two trigger points (Trigger-1 and Trigger-2) are installed 61.5 *cm* apart in the shock tube to measure the incident wave Mach number. Similarly other four trigger points are also installed at different positions by the supporting rod, shown in **Figure 6**, in the open atmosphere to calculate the wave speeds during the propagation in the open atmosphere and the calculated traveling time between different triggers are recorded. Trigger-2 is installed at the end point of the shock tube where $x = 0.0$ *cm* and all other trigger distances are measured from Trigger-2. Here the distance of the Trigger-3 from Trigger-2 is 9 *cm*, shown in **Figure 6-7**. Similarly from Trigger-2, the distance of

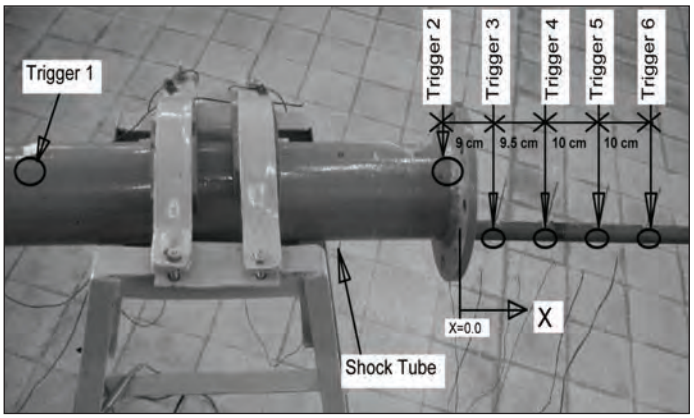

Figure 6: A schematic illustration of the horizontal shock tube where the relative distances between different trigger points are given

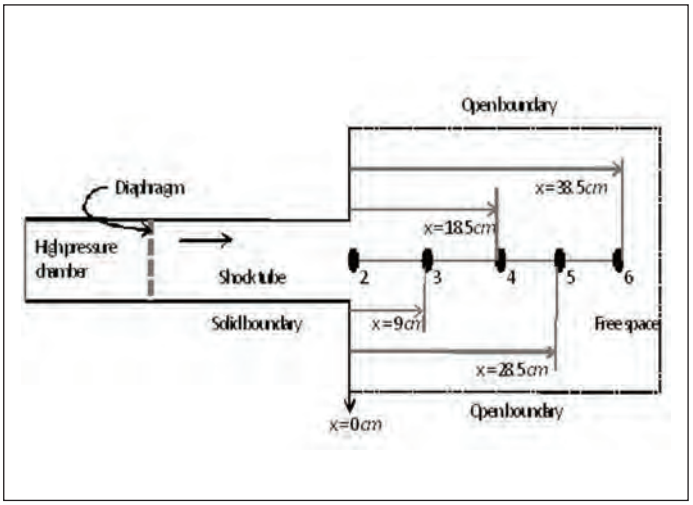

Figure 7: Schematic diagram of the Shock tube and the position of trigger points

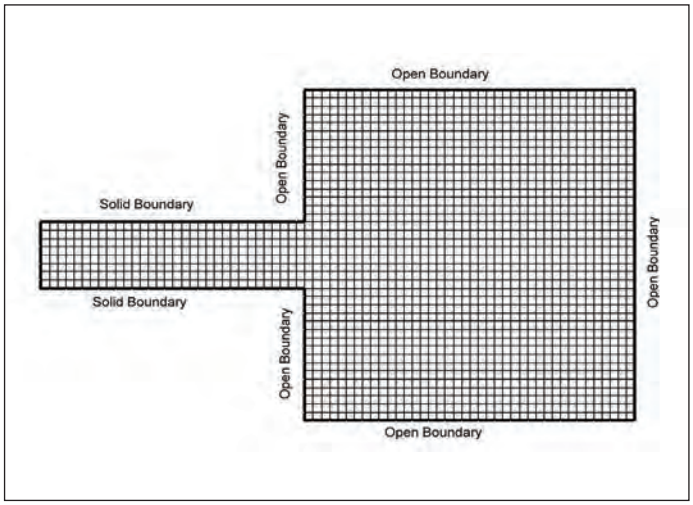

Figure 8: 2D numerical grids of the shock tube and the free space where solid boundaries are taken for shock tube and open boundaries are taken for free space

Trigger-4 is 18.5 *cm*, the distance of Trigger-5 is 28.5 *cm* and the distance of Trigger-6 is 38.5 *cm* respectively which are shown in **Figure 6-7**.

3.0 NUMERICAL SIMULATION

3.1 Problem Specifications

In the present simulation, the results obtained by solving two-dimensional (2D) Euler equations are used to compare with experimental results. The valid 2D numerical code has been developed to solve the Euler equations for the shock wave propagation in the open atmosphere and the extended 3D code was used by Jinnah and Takayama [1] to compute the outcomes of the shock/turbulence interaction. The governing equation is,

$$\frac{\partial Q}{\partial t}+\frac{\partial F}{\partial x}+\frac{\partial G}{\partial y}=0$$

Where $Q = [\rho, \rho u, \rho v, e]$,

$$F = [\rho u, \rho u^2, \rho uv, u(e+p)],$$

$$G = [\rho v, \rho uv, \rho v^2, v(e+p)]$$

Here Q is the vector of conservative variables which contains mass, momentum and energy. All variables are calculated in per unit volume. ρ is taken as the mass per unit volume. Two momentum terms in two-dimensional Cartesian coordinates system are ρu, and ρv per unit volume. F and G are the two inviscid flux vectors in x- and y- axis respectively. Each flux vectors contain mass flux, momentum flux and energy flux. ρu is the mass flux and ρu^2, ρuv are the momentum flux and $u(e+p)$ is the energy flux in the x-axis. Similarly ρv is the mass flux and ρuv, ρv^2 are the momentum flux and $v(e+p)$ is the energy flux in the y-axis. Also ρ is the fluid density and u, v are velocity components in each direction of Cartesian coordinates. While e is the total energy per unit volume, pressure p can be expressed by the following state equation for ideal gas

$p=(\gamma-1)[e-\frac{1}{2}\rho(u^2+v^2)]$ where γ is the ratio of specific heats.

The governing equation described above for compressible inviscous flow is discretised by the finite volume method. A second order, upwind Godunov scheme of Flux vector splitting method is used to discrete the inviscid flux terms where HLL-Reimann solver is used for shock capturing in the flow. Two dimensional cells with adaptive grid systems are used for these computations.

The initial two-dimensional grid systems are shown in **Figure 8**. The physical size of each cell before adaptation is equal to 13 x 13 (*mm*). The grid adaptation is one of the improved and computational time saving techniques, which is used in these computations. The grid adaptation is performed by two procedures, one is refinement procedure and another is coarsening procedure. The refinement and coarsening operations are handled separately in computation.

3.2 Boundary Conditions

The upstream of incident shock wave is set as inflow boundary condition, the properties and velocities of which are calculated from Rankine-Hugoniot conditions with incident shock Mach number. The downstream inflow boundary conditions, shown in **Figure 8**, are open boundary conditions and the wall surfaces of the shock tube are used as solid boundary where the gradients normal to the surface are taken zero.

4.0 RESULTS AND DISCUSSION

In the present research work, the investigation on wave propagation in the open atmosphere from the end section of the shock tube is focused mainly to observe the decay of the wave strength. Both experimentally and numerically, the decay of the wave strength measures during propagation and finally a comparison test is performed between numerical results and experimental results. The numerical images are used to visualize the density contour in the flow field during the shock wave propagation in the open atmosphere. It is observed from the density contour of the wave that the number of lines near shock front decreases gradually as increasing the distance of the shock front from the end section of the shock tube. The density contour behind the shock front shows that each line indicates the uniform density along the line and the two adjacent lines

measure the density gradient of the flow field. Here there have approximately 60 contour lines considered between maximum and minimum density in the field and the density contours step is 0.01 which are shown in **Figure 9(i)–(viii)**. Similarly the density fringes are visualized numerically to investigate the wave propagation phenomena in the open atmosphere which are shown in **Figure 10(i)–(viii)**. Many researchers used Double exposure holographic interferometry to visualize experimentally the density fringes for the shock wave interaction with different objects, like Wedge, Cone and Cylinder etc. Other researchers used Laser beam to take two consequent exposures on the same photo film within few nanoseconds. Because of double shot on the same photo film, the word double exposure was used. Numata *et al*. [5] conducted their experiments to observe the shock wave reflection from a skewed wedge by using the holographic interferometry. A series of experiments was carried out in order to investigate the initial transient flow in the nozzle by Saito *et al*. [6]. In their experiment the flow was visualized by using the double exposure laser holographic interferometry and a comparison test was conducted on density fringes of the flow field obtained by experimentally and numerically. In the present computation, the density fringes are used to explain the wave propagation characteristics and to get the complete idea on the spherical expansion of the shock front in the open atmosphere.

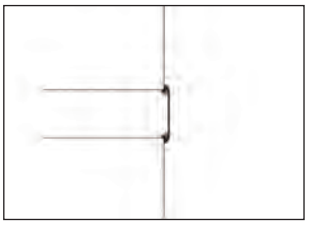

(i) Near end section of the shock tube, $x = 0$ *cm*, density contours step 0.01

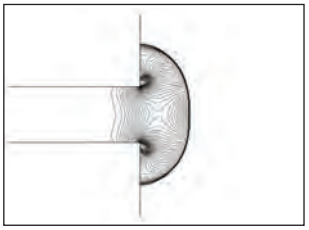

(ii) Shock front position at $x = 9.0$ *cm*, density contours step 0.01

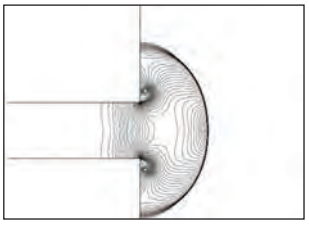

(iii) Shock front position at $x = 13.75$ *cm*, density contours step 0.01

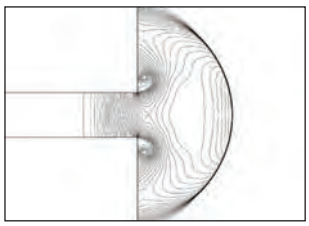

(iv) Shock front position at $x = 18.5$ *mm*, density contours step 0.01

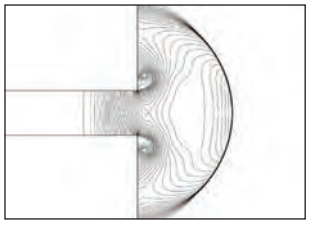

(v) Shock front position at $x = 23.5$ *mm*, density contours step 0.01

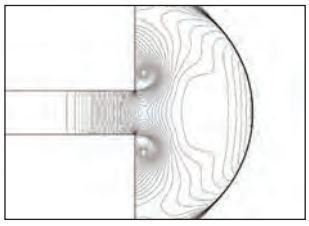

(vi) Shock front position at $x = 28.5$ *mm*, density contours step 0.01

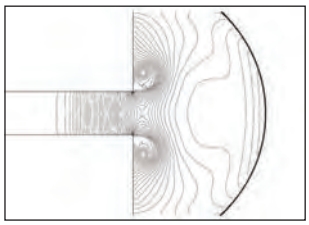

(vii) Shock front position at $x = 33.5$ *mm*, density contour step 0.01

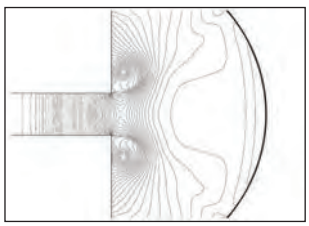

(viii) Shock front position at $x = 38.5$ *mm*, density contour step 0.01

Figure 9: Numerical results of the density fringes at different locations of the shock front in the open Atmosphere for moderate shock propagation

(i) Near end section of the shock tube, x = 0.0 *cm*, density fringes step 0.1

ii) Shock front position at x = 9.0 *cm*, density fringes step 0.1

(iii) Shock front position at x = 13.75 *cm*, density fringes step 0.1

(iv) Shock front position at x = 18.5 *cm*, density fringes step 0.1

(v) Shock front position at x = 23.5 *cm*, density fringes step 0.1

(vi) Shock front position at x = 28.5 *cm*, density fringes step 0.1

(vii) Shock front position at x = 33.5 *cm*, density fringes step 0.1

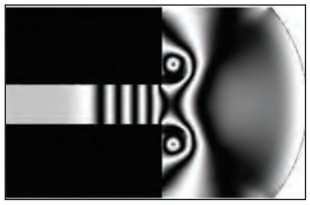

(viii) Shock front position at x = 38.5 *cm*, density fringes step 0.1

Figure 10: Numerical results of the density fringes at different locations of the shock front in the open Atmosphere for moderate shock propagation

The present time measuring technique is used successfully in experiment to investigate the wave propagation in the open atmosphere. The sensing point-1 as shown in **Figure 5**, is installed at the end section of the shock tube where at trigger-2, *x = 0 cm*, shown in **Figure 7**. Similarly sensing point-2, shown in **Figure 5**, is installed at a point in the free space where the distance from the end section of trigger-3 *is x = 9 cm*, shown in **Figure 7**. During the wave propagation over these triggers, the device is captured frequency which is directly proportional to the travelled time of the wave from trigger-2 to trigger-3. The captured frequency is converted into travelled time by dividing the known crystal frequency. Here the known crystal frequency is 3579540 Hz, that means, 1 second is equivalent to 3579540 pulses. Similarly by installing sensing point-1 and sensing point-2 of the device at the points where trigger-2, *x = 0 cm* and trigger-6, *x = 38.5 cm* respectively, the captured frequency is recorded during the wave propagation between these trigger points and the captured frequency is then converted into travelled time of the wave.

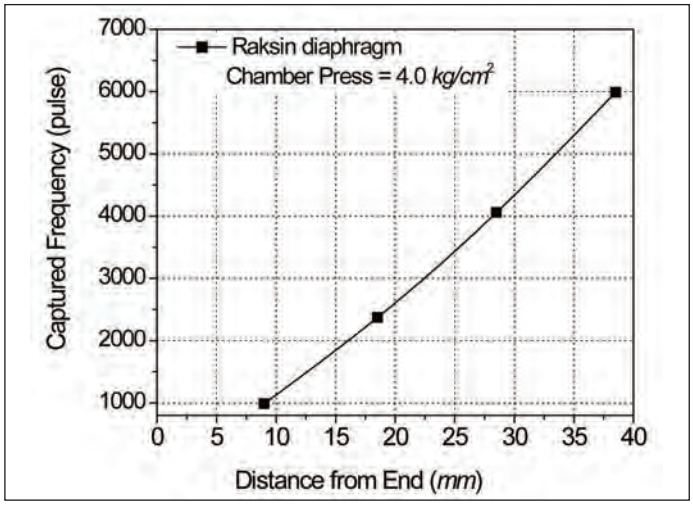

Figure 11: Captured frequency recorded experimentally during the wave travels between different trigger points in the open Atmosphere (Here 1 sec = 3579540 pulses)

Figure 11 shows captured frequencies recorded experimentally during the wave propagation over the points in the open atmosphere where the position of the trigger points are, *x = 0 cm*, *x = 9 cm*, *x = 18.5 cm*, *x = 28.5 cm* and *x = 38.5 cm*, shown in **Figure 7** and here Raksin sheet is used as a diaphragm in the shock tube. The average wave speeds (U_{av}) are determined by the ratio of the distance between two trigger points to the wave travelled time of this distance and the wave speed between any two trigger points is considered as the wave speed at the mid point of the two trigger points. In case of Raksin diaphragm, **Figure 12** shows the average wave speed (U_{av}) variations from the end of the shock tube in the open atmosphere. Here the maximum wave speed is *326 m/s* at position, *x = 4.5 cm* which is the mid point between the trigger points, *x = 0 cm* and *x = 9 cm*. As compare to the local sound velocity, the wave speed is subsonic. So it is concluded that the rupture of the Raksin diaphragm generates subsonic wave at the end point of the shock tube and as increasing the travel distance by the wave, the wave strength decreases during propagation in the open atmosphere which is shown in **Figure 12**.

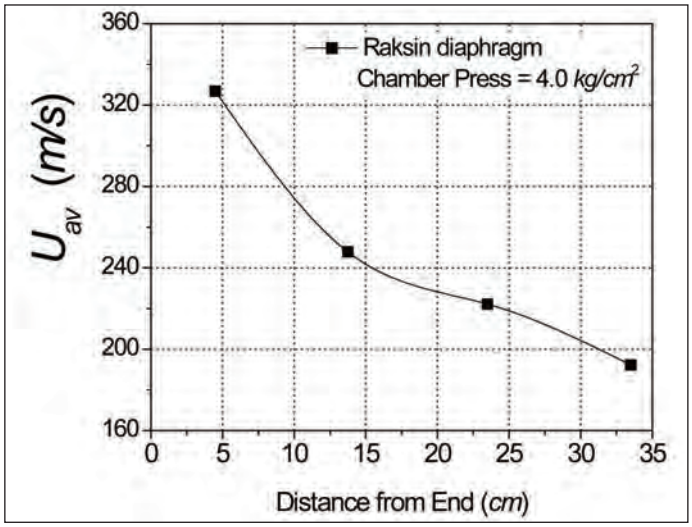

Figure 12: Experimental results of the average wave speed at different locations of the shock front in the open Atmosphere (Here rupture of Raksin diaphragm generates subsonic wave at the end of shock tube)

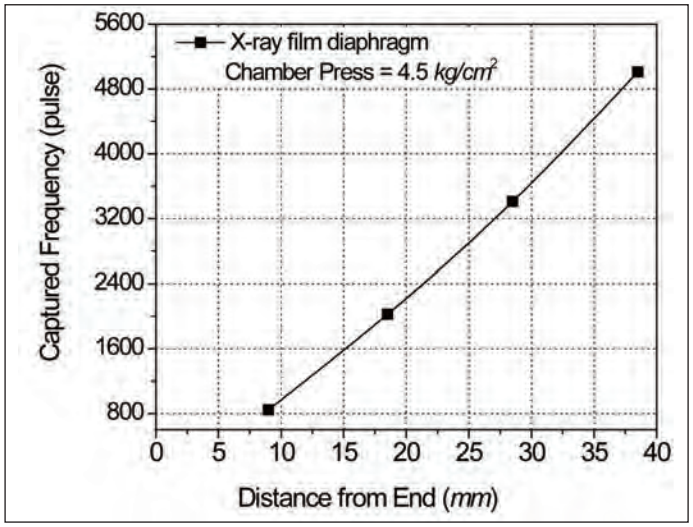

Figure 13: Captured frequency recorded experimentally during the wave travels between different trigger points in the open Atmosphere (Here 1 sec = 3579540 pulses)

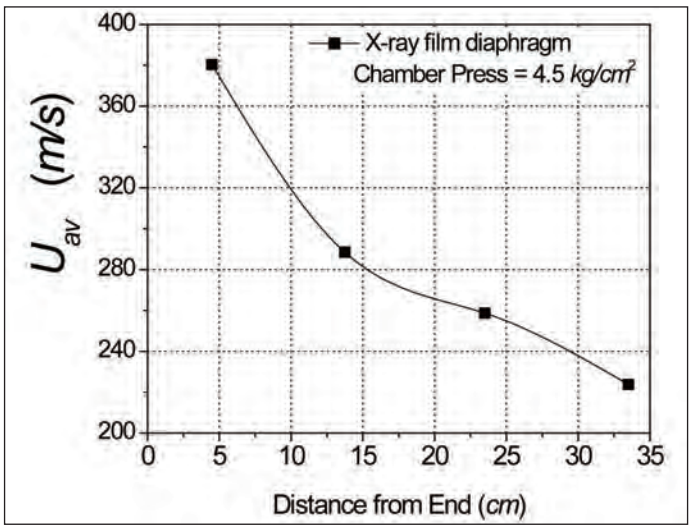

Figure 14: Experimental results of the average wave speed at different locations of the shock front in the open Atmosphere (Here rupture of used X-ray film diaphragm generates supersonic wave at the end of shock tube)

Similarly **Figure 13** shows captured frequencies recorded experimentally during the wave propagation over the points in the open atmosphere where the position of the trigger points are *x = 0 cm*, *x = 9 cm*, *x = 18.5 cm*, *x = 28.5 cm* and *x = 38.5 cm*, shown in **Figure 7** and here used X-ray film is used as a diaphragm in the shock tube. In case of used X-ray film, **Figure 14** shows the average wave speed (U_{av}) variations from the end of the shock tube in the open atmosphere. Here the maximum wave speed is *380 m/s* at position, *x = 4.5 cm* which is the mid point between the trigger points, *x = 0 cm* and *x = 9 cm*. As compare to the local sound velocity, the wave speed is supersonic. So it is concluded that the rupture of the used X-ray film diaphragm generates shock wave at the end point of the shock tube and as increasing the travel distance by the wave, the shock wave strength decreases to subsonic wave during propagation in the open atmosphere which is shown in **Figure 12**.

The decay of the wave propagation is determined both experimentally and numerically during the wave propagation over the trigger points in the open atmosphere and **Figure 15** shows the profile of the percentage of decay at different trigger points when Raksin sheet is used as a diaphragm in the shock tube. It is observed that initially the percentage of decay increases obtained by experiment as compare to the numerical results. It is observed that the percentage of the decay increases as increasing the distance from the end point of the shock tube. It is also observed that the decay obtained from experiment has the good agreement with the numerical results.

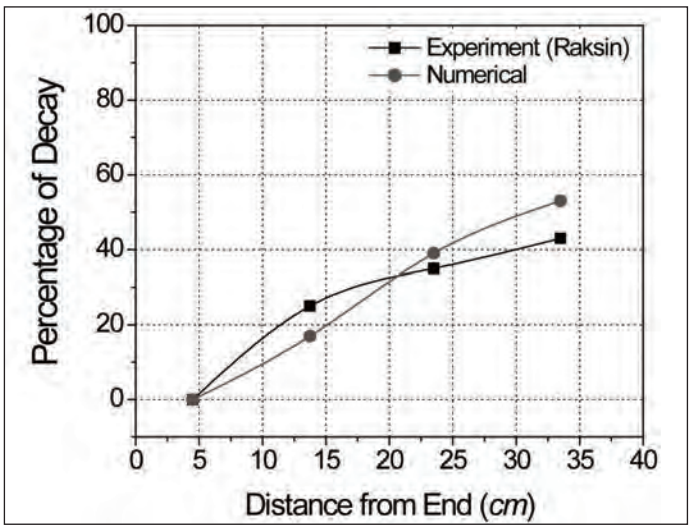

Figure 15: Comparison between Experimental results and Numerical results of the percentage of decay of the wave propagation in the open Atmosphere (Here rupture of Raksin diaphragm generates subsonic wave at the end of shock tube)

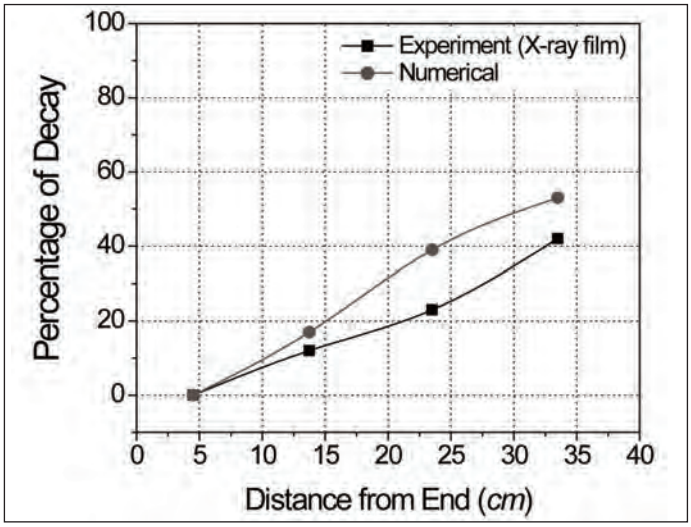

Figure 16: Comparison between Experimental results and Numerical results of the percentage of decay of the wave propagation in the open Atmosphere. (Here rupture of used X-ray film diaphragm generates supersonic wave at the end of shock tube)

Figure 16 shows the profile of the percentage of decay at different trigger points when used X-ray film is used as a diaphragm in the shock tube. It is observed that initially the percentage of decay decreases obtained by experiment as compare to the numerical results. It is observed that the percentage of the decay increases as increasing the distance from the end point of the shock tube. It is also observed that the decay obtained from experiment has the good agreement with the numerical results. So it is concluded that the decay of subsonic wave and supersonic wave has the same nature during the propagation in the open atmosphere and such type of decay observes due to spherical expansion of the wave in the open atmosphere. The decay of shock wave may differ with subsonic wave due to rapid compression and expansion happened during shock wave propagation but the percentage of decay is same after propagating far distance in the open atmosphere.

5.0 CONCLUSION

In the present experimental works, shock wave has been generated by rupturing different types of diaphragms in the shock tube. The rupturing properties of diaphragm are the major factors to generate shock wave in the shock tube. It is observed that used X-ray film gives the better performance as compare to Raksin sheet for rupturing purposes and the properties like toughness and brittleness are the best properties of the diaphragm.

For calculating the wave speed in the open atmosphere, the present time measuring technique is simple in use and accurate in measurement as compare to other complicated technique like wave visualization technique. During the wave propagation in the open atmosphere, the wave speed decreases as increasing the travel time. So decreasing the wave speed indicates that the decay of the wave strength is the normal phenomenon during propagation in the open atmosphere. In the present research, the decay of the wave strength obtained from experimental results has the good agreement with numerical results. ■

REFERENCES

[1] Jinnah MA and Takayama K. (2011) Numerical and Experimental Study of Shock/Turbulent Flow Interaction – A Code Validation Test. Journal IEM, Vol. 72, No.4: 37-46.

[2] Doig GC, Barber TJ, Leonardi E, Neely J and Kleine H. (2008) Methods for investigating supersonic ground effect in a blowdown wind tunnel, Shock Waves, 18: 155-15.

[3] Kobiera A, Szymczyk J, Wola'nski P and Kuhl A. (2009) Study of the shock-induced acceleration of hexane droplets, Shock Waves, 18: 475-85.

[4] Pianthong K, Zakrzewski S, Behnia M and Milton BE. (2002) Supersonic liquid jets: Their generation and shock wave characteristics, Shock Waves, 11: 457-66.

[5] Numata D, Ohtani K and Takayama K. (2009) Diffuse holographic interferometric observation of shock wave reflection from a skewed wedge, Shock Waves, 19: 103-112.

[6] Saito T and Takayama K. (1999) Numerical simulations of nozzle starting process, Shock Waves, 9: 73-79.

PROFILES

DR MOHAMMAD ALI JINNAH is an Associate Professor in Department of Mechanical and Chemical Engineering, Islamic University of Technology (An Organ of the OIC), Bangladesh. He obtained his Ph.D. from Tohoku University, Sendai, Japan in 2005 specialising in Shock Wave interaction with turbulent flow.

MR. MOHAMMAD MONJURUL EHSAN is a Lecturer in Department of Mechanical and Chemical Engineering, Islamic University of Technology (An Organ of the OIC), Bangladesh. He obtained his M.Sc. Engg degree from IUT in 2012 specialising in Shock Wave propagation in Open Atmosphere.